InGaAsP/InP Membrane Gain Sections for III-V/SiN_x Heterogeneous Photonic Integration

Christopher Heidelberger[1], Christos T. Santis[2], Jason J. Plant[1], Erin M. Morissette[1], Dave Kharas[1], Reuel B. Swint[1], Amnon Yariv[2], Paul W. Juodawlkis[1]
[1]*Lincoln Laboratory, Massachusetts Institute of Technology, Lexington, Massachusetts 02420, USA*
[2]*Department of Applied Physics and Materials Science, California Institute of Technology, Pasadena, California, 91125, USA*
Author e-mail address: c.heidelberger@ll.mit.edu

Abstract: We present a fabrication process for 200 nm thick InGaAsP/InP membrane gain sections (λ = 1550 nm) suitable for heterogeneous integration with SiN_x PICs. The structures exhibit desired electrical performance and support lasing.

1. Introduction

Photonic integrated circuits (PICs) using silicon nitride (SiN_x) or other dielectric waveguides offer benefits over more conventional silicon (Si) waveguides, including lower loss, better power handling, and broader wavelength transparency [1]. Heterogeneous integration (*i.e.*, surface bonding) of III-V semiconductors with Si PICs allows for parallel fabrication of multiple gain sections [2]. However, this approach has not been successfully demonstrated with SiN_x PICs due to the low refractive index of SiN_x relative to the III-V materials, which makes it difficult to couple light evanescently from III-V into SiN_x. Thin III-V membrane lasers with lateral current injection have been demonstrated on Si substrates [3,4]. With such a structure, it is possible to engineer an adiabatic transition from a III-V fundamental mode into a SiN_x waveguide using a III-V taper with modest tip width. In this work, we develop a fabrication process for an InGaAsP/InP electrically-pumped gain section (1550 nm) suitable for integration with SiN_x PICs (Figure 1a), demonstrating progress towards fabrication of hybrid III-V/SiN_x lasers and other integrated systems.

2. Device Fabrication

The InGaAsP/InP multi-quantum well (MQW) structure was grown on InP substrates by metalorganic chemical vapor deposition (MOCVD) with the following layers: a 50 nm sacrificial InGaAs etch stop, a 50 nm InP bottom clad, a 100 nm InGaAsP MQW region with five 0.4% compressively strained wells having peak photoluminescence at 1550 nm, and a 50 nm InP top clad. For process development, surrogate SiN_x PICs (with no SiN_x layer) were prepared by plasma-enhanced chemical vapor deposition (PECVD) deposition of SiO_2 on a Si substrate followed by chemical-mechanical polishing (CMP) to a final SiO_2 thickness of 3 µm with an RMS roughness of 400 pm. The III-V wafer was then bonded to the surrogate PIC. O_2 plasma is frequently used to prepare surfaces prior to covalent oxide-oxide bonding [5]. However, in this case O_2 plasma processing was found to cause significant degradation of carrier lifetime in the InGaAsP MQW (Figure 1b) due to the close proximity of the MQW layers to the III-V surface. UV-ozone pre-treatment was chosen because of its reduced impact on carrier lifetime and sufficient strength of the resulting oxide-oxide bond. Figure 1c shows an image of the sample after chemical substrate and etch stop removal, showing the high bond yield (>95%) and low defect density (~75 cm^{-2}). Next, the InP top clad and InGaAsP MQW layers were patterned into stripes using a 400 nm thick SiN_x hardmask, leaving behind the InP bottom clad. 150 nm of undoped InP was grown selectively by MOCVD on either side of the stripe. Cross-section SEM shows complete filling of the undercut regions with regrown InP (Figure 1d and e). Both <011> stripe orientations were investigated, with the [011] direction being preferred due to nearly vertical InGaAsP MQW sidewalls. Si+ and Be+ ion implants were used to define the n-

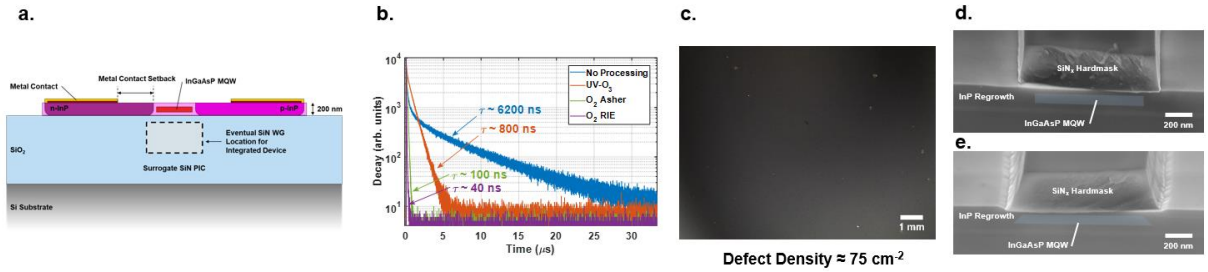

Figure 1: a) Lateral cross-section schematic of InGaAsP/InP membrane gain section showing location of SiN_x waveguide for heterogeneous integration. Note that the SiN_x waveguide is not present in this work. b) TRPL decay of InGaAsP/InP MQW structure before and after various pre-bond surface treatments. c) Image of bonded III-V membrane after InP substrate removal showing large bonded area and low defect density. d) Cross-section SEM of patterned InGaAsP MQW (highlighted) surrounded by InP regrowth with ridge in [011] direction. e) Same as (d) but with ridge in [0-11] direction.

and p-type lateral contact regions, respectively. For both implants, the SiN_x hardmask acted as a self-aligned implant barrier over the MQW stripe resulting in a doping setback of ~100 nm from the MQW region (see Figure 1d). Ohmic contacts were then deposited. A standard Ni/Ge/Au metallurgy was used for the n-type contacts while a Au/Zn/Au metallurgy was used for the p-type contacts. Transmission line measurements (TLM) showed sheet resistances of 3380 Ω/sq and 180 Ω/sq and contact resistivities of 7×10^{-6} Ω cm^2 and 5×10^{-5} Ω cm^2 for n- and p-type InP contacts, respectively. Finally, the InP membrane was removed from the area surrounding the devices. Most devices included InP tapers at each end of the InGaAsP MQW stripe, which will enable an adiabatic transition into an underlying SiN_x waveguide in a future iteration. Others included abrupt etched InP facets to form Fabry-Perot lasers in the III-V for testing purposes.

3. Device Testing

I-V data from a 5 mm long InGaAsP/InP membrane gain section with tapered ends and a 2 µm metal setback is shown in Figure 2a. The I-V behavior closely follows simulated data of the nominal structure (self-consistent solution of Poisson, drift, and diffusion equations) indicating that the dopant concentrations and setback distances from the MQW stripe are as-targeted. Series resistance scaled as expected with varying metal setback distances (1.2 Ω for 1 µm setback to 3.3 Ω for 3 µm setback). Top-down images of the spontaneous emission show uniform power along the length of the device indicating uniform electrical injection and recombination mechanics. Figure 2b shows one such image and Figure 2c shows the relative power as a function of position along the InGaAsP MQW stripe. Devices having abrupt rather than tapered ends exhibited lasing behavior (Figure 2d) with a threshold current density per quantum well of ~380 A/cm^2. This high value is not unexpected given the relatively low 0.4% compressive strain in the quantum wells [6] and low reflectivity of the etched facets, and is comparable to that demonstrated in similar membrane lasers [3].

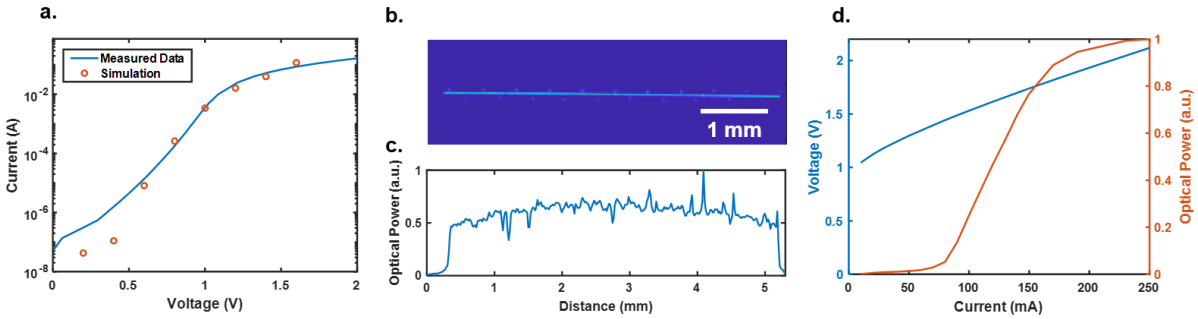

Figure 2: a) I-V curve for a 5 mm long device compared to simulation of nominal structure assuming 5000 cm/s InP surface recombination velocity. b) Top-down IR image of spontaneous emission from a 5 mm long device under 100 mA drive current. V-shaped spots along top and bottom of stripe are caused by light scattering from electrical probe tips. c) Relative optical power along length of device from (b). d) L-I-V data from 5 mm long InGaAsP/InP membrane laser.

4. Conclusion

We have developed a process for fabrication of InGaAsP/InP membrane gain sections on SiO_2/Si substrates compatible with heterogeneous integration with SiN_x PICs. The resulting devices exhibit good electrical performance, consistent with simulation, indicating good material quality and correct geometry. Devices without end mirrors showed uniform spontaneous emission along their length and devices with end mirrors exhibited room-temperature CW lasing.

DISTRIBUTION STATEMENT A. Approved for public release. Distribution is unlimited. This material is based upon work supported by the Defense Advanced Research Projects Agency (DARPA) under Air Force Contract No. FA8702-15-D-0001. Any opinions, findings, conclusions or recommendations expressed in this material are those of the author(s) and do not necessarily reflect the views of DARPA.
Delivered to the U.S. Government with Unlimited Rights, as defined in DFARS Part 252.227-7013 or 7014 (Feb 2014). Notwithstanding any copyright notice, U.S. Government rights in this work are defined by DFARS 252.227-7013 or DFARS 252.227-7014 as detailed above. Use of this work other than as specifically authorized by the U.S. Government may violate any copyrights that exist in this work.

5. References

[1] C. Sorace-Agaskar *et al.*, "Versatile Silicon Nitride and Alumina Integrated Photonic Platforms for the Ultraviolet to Short-Wave Infrared," *IEEE J Quantum Elect*, vol. 25, no. 5, pp. 1–15 (2019)
[2] T. Komljenovic, D. Huang, P. Pintus, M. A. Tran, M. L. Davenport, and J. E. Bowers, "Photonic Integrated Circuits Using Heterogeneous Integration on Silicon," *Proc IEEE*, vol. 106, no. 12, pp. 2246–2257 (2018)
[3] S. Matsuo, T. Fujii, K. Hasebe, K. Takeda, T. Sato, and T. Kakitsuka, "Directly modulated buried heterostructure DFB laser on SiO_2/Si substrate fabricated by regrowth of InP using bonded active layer," *Opt Express*, vol. 22, no. 10, p. 12139 (2014)
[4] T. Fujii *et al.*, "Evaluation of Device Parameters for Membrane Lasers on Si Fabricated with Active-Layer Bonding Followed by Epitaxial Growth," *IEICE T Electron*, vol. E100.C, no. 2, pp. 196–203 (2017)
[5] M. Yokoyama *et al.*, "Formation of III–V-on-insulator structures on Si by direct wafer bonding," *Semiconductor Sci Tech*, vol. 28, no. 9, p. 094009 (2013)
[6] A. R. Adams, "Strained-Layer Quantum-Well Lasers," *IEEE J Quantum Elect*, vol. 17, no. 5, pp. 1364–1373 (2011)